Coherent Operations and Screening in Multielectron Spin Qubits

A. P. Higginbotham,[1,2] F. Kuemmeth,[2] M. P. Hanson,[3] A. C. Gossard,[3] and C. M. Marcus[2]

[1]*Department of Physics, Harvard University, Cambridge, Massachusetts 02138, USA*
[2]*Center for Quantum Devices, Niels Bohr Institute, 2100 Copenhagen, Denmark*
[3]*Materials Department, University of California, Santa Barbara, California 93106, USA*

Multielectron spin qubits are demonstrated, and performance examined by comparing coherent exchange oscillations in coupled single-electron and multielectron quantum dots, measured in the same device. Fast (> 1 GHz) exchange oscillations with a quality factor $Q \sim 15$ are found for the multielectron case, compared to $Q \sim 2$ for the single-electron case, the latter consistent with experiments in the literature. A model of dephasing that includes voltage and hyperfine noise is developed that is in good agreement with both single- and multielectron data, though in both cases additional exchange-independent dephasing is needed to obtain quantitative agreement across a broad parameter range.

Spin-1/2 quantum dots with controlled exchange coupling form a potentially powerful platform for manipulating quantum information [1]. Single electrons confined by electrostatic gates in semiconductors are a well-developed realization of this system, and meet many of the basic requirements of quantum information processing. A broad research effort has emerged under this approach, focused on materials such as GaAs [2–4], carbon nanotubes [5], InAs [6,7], InSb [8], and Si [9,10]. In each system, producing large numbers of single-electron quantum dots places severe demands on materials and device design, and is a considerable obstacle to scalability [11]. Moving from single confined electrons to multielectron qubits alleviates these difficulties, and, as we show, can also improve performance.

Requirements for conventional spin qubits include a spin-1/2 ground state, and a gap to excited states larger than temperature and the energy scales associated with control and coupling. For realistic densities, interactions are relatively weak, typically (though not always) resulting in a spin-1/2 ground state for odd occupancy [12]. Multielectron dots can have higher-spin ground states and smaller-than-average gaps to the first excited state, due for instance to accidental degeneracies in their excitation spectrum. This concern may partially explain why there have been relatively few studies of their use as spin qubits. In practice, however, such degeneracies are typically lifted by desymmetrizing the confining potential or changing the applied magnetic field [13,14].

Previous experimental work on multielectron quantum dots has demonstrated Pauli blockade [15–21] and coherent operation [7]. In single-electron dots, both nuclear [22,23] and electrical [24,25] dephasing have been characterized, with electrical noise modeled as a fluctuating detuning between double-dot levels. Multielectron quantum dots have also received theoretical attention due to ease of realization as well as possibly improved performance [13,14,26–28].

In this Letter, we investigate coherent exchange oscillations in coupled multielectron GaAs quantum dots—this operation was specifically chosen to be sensitive to electrical noise—and compare results to oscillations in the same device operated with single-electron dots. Our primary finding is that multielectron qubits can be operated analogously to the single-electron case, which alleviates the need for singly occupied dots. We also find significantly improved coherence in the multielectron case, consistent with expectations of screening by core electrons [14,26]. By analyzing the dephasing during the exchange-gate operation, we characterize the electrical noise environment for each occupancy. For both single and multiple occupancies, voltage noise affecting the detuning between dots dominates dephasing for large exchange, and fluctuating hyperfine (Overhauser) fields dominate dephasing for small exchange. For a range of intermediate exchange, an exchange-independent dephasing mechanism of unknown origin is dominant. The upshot of this work is that one can simultaneously relax fabrication requirements and improve qubit performance by working in the multielectron regime.

We report measurements on a double quantum dot with integrated charge sensor, formed by Ti/Au depletion gates patterned by electron beam lithography on the surface of a GaAs/Al$_{0.3}$Ga$_{0.7}$As heterostructure with two-dimensional electron gas (2DEG) of density $\sim 2 \times 10^{15}$ m^{-2} and mobility 20 m^2/V s, located 100 nm below the wafer surface.

The charge configuration of the double dot is detected using a conductance measurement of a proximal quantum dot [Fig. 1(a)] [29]. All measurements are performed in a dilution refrigerator with an electron temperature of ~ 50 mK. A sufficiently large in-plane magnetic field is applied to isolate the $m_S = 0$ subspace of the double dot Hamiltonian. Specific values of field are given for particular data sets, with no observed dependence on the value of field the range 50–200 mT.
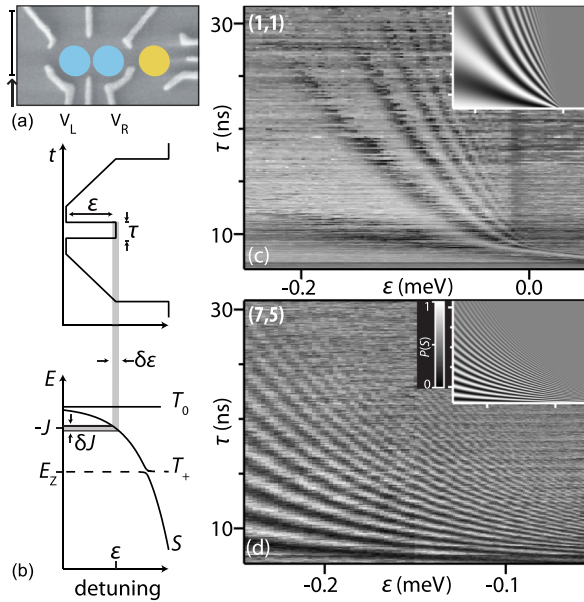
FIG. 1 (color online).   (a) Scanning electron micrograph of a lithographically identical device, indicating double dot (blue) and charge sensor (yellow). Scale bar indicates 500 nm, arrow indicates magnetic field direction [200 mT for (1,1), 50 mT for (7,5)] and the [110] crystal axis. (b) Schematic exchange pulse sequence. An adiabatic ramp to $J = 0$ initializes the system in the lowest energy $m_S = 0$ eigenstate before an exchange pulse of duration τ to detuning ε is applied. Detuning noise $\delta\varepsilon$ induces exchange fluctuations δJ, which limits the number of visible exchange oscillations at high detuning. (c) Probability of detecting a singlet $P(S)$ as a function of detuning and exchange time for single-electron dots. (d) Same as (c) but for multielectron dots. Coherence is significantly improved for the multielectron exchange case. Insets: Simulated exchange oscillations (see text). Color scale shared for all 2D plots.

Negative voltages were applied to the gate electrodes in order to form two quantum dots with several GHz of tunnel coupling. Plunger gate voltages V_L and V_R control electron occupancy in the left and right dots, denoted n, m, and also control interdot tunneling via the detuning $\varepsilon \propto (V_L - V_R)$. When each dot forms a spin-1/2 system, tunneling occurs only between singlet-correlated dots due to Pauli blockade. The result is that the singlet (S) state can lower its energy with respect to the triplet (T_0) by an exchange energy J [cf. Fig. 1(b)]. When these states are split by J, the device is in a superposition of different charge states, and is therefore susceptible to electrical noise.

To set up the exchange oscillation measurement, an adiabatic ramp to $J = 0$ maps the initialized S state to the lower zero-spin eigenstates of the Overhauser nuclear field [see Fig. 1(b)]. Next, a square exchange pulse applied to ε turns on exchange $J(\varepsilon)$ for a time τ, accumulating a phase of $2\pi J(\varepsilon)\tau$ between S and T_0. In terms of the $J = 0$ eigenstates, this phase accumulation corresponds to oscillations between the ground and excited state at frequency of J. Finally, the $J = 0$ eigenstates are mapped via a reverse

ramp onto S and T_0, which project differently into charge states of the double dot, resulting in a different sensor dot conductance.

By varying ε and τ, and repeating the cycle for > 10 min to average over the nuclear and electrical fluctuations, we generate a family of oscillating curves for the device configured with single [Fig. 1(c)] and multiple [Fig. 1(d)] electrons. The sensor conductance was normalized to 1 at its first maximum and 1/2 at its settling value such that it reflects a singlet return probability, $P(S)$.

Our central result is that not only are exchange oscillations observed between multiply occupied dots, showing that a multielectron dot forms a good qubit, but that the quality of these oscillations is improved over the singly occupied case. This is shown in Fig. 1, where we observe high-quality exchange oscillations between multielectron dots that clearly outperform the single-electron case in the same device. We have examined exchange gates between multielectron dots at different electron-number occupations for three different cooldowns and two different devices with similar results (see Supplemental Material [32]).

We now examine the origin of the improvement observed in the multielectron exchange gate. We consider a model that includes several contributions to the total dephasing rate Γ, including ε-equivalent noise [Fig. 1(b)], which dominates at large J, ε-independent dephasing, which dominates at intermediate J, and dephasing due to random gradients in the Overhauser field in the z direction, which dominates for small J. We find that this model is sufficient to describe our observations over the entire parameter range of Fig. 1 (insets).

Exchange oscillations were fit with a decaying sinusoid of the form

$$\exp[-(\Gamma\tau)^2]\cos(2\pi J\tau + \varphi), \qquad (1)$$

with fit parameters Γ, J, and φ. A phase shift φ can arise from bandwidth limits in the apparatus. Exchange oscillations are well fit by this Gaussian envelope, and inconsistent with an exponential envelope, consistent with [25]. The form of this decay envelope has physical implications: an exponential envelope can indicate either Gaussian-distributed white noise or Lorentzian-distributed low-frequency noise in exchange. A Gaussian envelope, on the other hand, reflects Gaussian-distributed low frequency (compared to $1/\tau$) exchange noise [25,30].

Figure 2(a) shows extracted values of $J(\varepsilon)$ from the fits. For single-electron occupation, $J(\varepsilon)$ can be found in regions where oscillations are not visible from the position of the S-T_+ anticrossing. This anticrossing occurs when the Zeeman splitting $E_Z = g\mu_B B$ is equal to the exchange $J(\varepsilon)$ [see Fig. 1(b) for $J(\varepsilon) = |E_Z|$], resulting in a change of sensor conductance [color scale of inset diamond, Fig. 2(a)] due to leakage into the T_+ state. J is extracted assuming the bulk g factor $g = -0.44$.
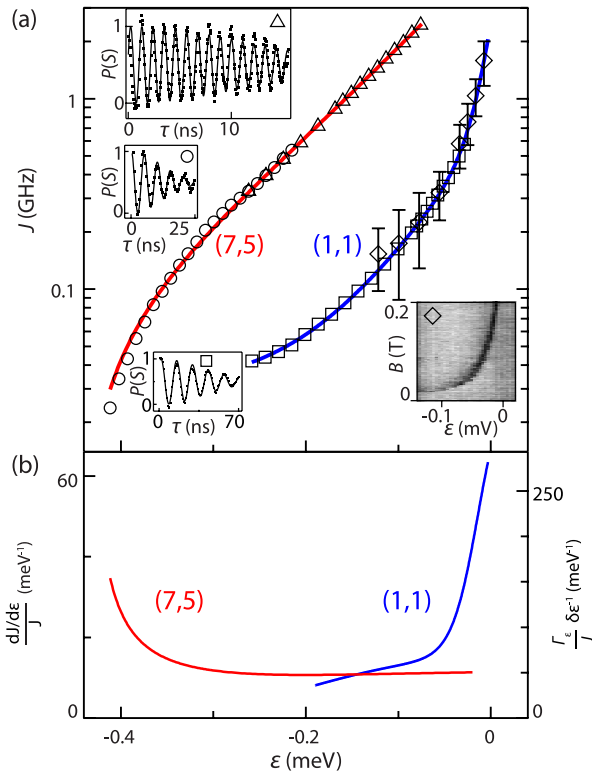
FIG. 2 (color online).   (a) Exchange coupling $J(\varepsilon)$ as a function of detuning ε for the single- and multielectron exchange gate. Data extracted from exchange oscillations (represented in insets) below (square, circle) and above (triangle) the range of the waveform generator (Tektronix AWG5014), measured by externally stepping the clock, and from the location of the S-T_+ anticrossing (diamond), where Zeeman and exchange energies are equal. Fits are to biexponential models (see text). (b) $(dJ/d\varepsilon)/J$, obtained numerically from the fits in (a), reflects the dephasing per exchange pulse due to ε noise. As ε approaches zero, the multielectron exchange gate should display improved coherence for equal amounts of ε noise. This is consistent with the observation of improved coherence in the multielectron case.

The component of dephasing attributable to fluctuations in detuning, denoted Γ_ε, depends on $dJ/d\varepsilon$, as illustrated in Fig. 1(b). For Gaussian low-frequency (compared to $1/\tau$) ε noise,

$$\Gamma_\varepsilon = \frac{dJ}{d\varepsilon}\pi\sqrt{2}\delta\varepsilon, \qquad (2)$$

where $\delta\varepsilon$ is the rms ε-equivalent noise [25,30]. To determine $dJ/d\varepsilon$, exchange profiles [Fig. 2(a)] were fit using a biexponential form, $A + B \exp[-k_1\varepsilon] + C \exp[-k_2\varepsilon]$. Figure 2(b) shows that as ε approaches zero, $(dJ/d\varepsilon)/J$ grows for the single-electron case, but saturates at a small value for the multielectron case, consistent with the screening of ε noise by core electrons. Thus, the shape of the exchange profile $J(\varepsilon)$ for the multielectron dots explains some immunity to ε-equivalent noise. However, at more negative detuning, Γ_ε for (1,1) falls below that of (7,5).

This is qualitatively inconsistent with our observations in Fig. 1(c) and suggests a deviation from the ε-equivalent noise model. The remainder of this Letter is concerned with developing a phenomenological noise model that describes our data.

We quantitatively examine the ε-noise model by extracting $\delta\varepsilon$ from our data. This can be done without assuming a particular functional form for $dJ/d\varepsilon$ by recasting Eq. (2) in integral form. Note that in the presence of only ε noise the number (quality) Q of observed oscillations satisfies the identity $J = Q\Gamma_\varepsilon$. Substituting Eq. 2 for Γ_ε and integrating both sides of this identity with respect to ε gives

$$\int J d\varepsilon = \pi\sqrt{2}\delta\varepsilon \int Q\frac{dJ}{d\varepsilon}d\varepsilon. \qquad (3)$$

Considering Q to be a function of J, these integrals can be rewritten

$$\int^{\varepsilon_i} J d\varepsilon = \pi\sqrt{2}\delta\varepsilon \int^{J(\varepsilon_i)} Q dJ. \qquad (4)$$

In Figs. 3(a) and 3(b) we numerically compute the integrals in Eq. (4) as a function of the upper-bound detuning point ε_i using the J and Q values from exchange oscillations in Fig. 2. A linear relationship reflects the dominant ε-equivalent noise, and the slope gives the noise strength. We find that the linear relationship between these integrals holds for large J, but not for intermediate and small J where other sources of dephasing dominate.

The measured dephasing rates $\Gamma(J)$ are shown in Figs. 3(c) and 3(d) for single- and multielectron cases. The deviation of $\Gamma(J)$ from the detuning-noise-only component $\Gamma_\varepsilon(J)$ is evident for both the single- and multielectron exchange operation. We next account for contributions to dephasing from fluctuations in the hyperfine field gradient Γ_n, determined independently from measured dephasing time $T_{2,n}^*$ in a diabatic singlet-separation measurement, following the analysis in Ref. [31] (see Supplemental Material [32]). The formula we use for Γ_n is valid for $J \gtrsim 1/T_{2,n}^*$. In the limit of $J \ll 1/T_{2,n}^*$, Γ_n decreases in proportion to J, as can be verified by explicitly integrating over the nuclear ensemble. This behavior is due to the following physical effect: nuclear fluctuations larger than J stop phase accumulation, but do not cause dephasing. Thus, when J becomes small, random Overhauser field gradients cause the visibility of oscillations to go to zero but do not contribute more noise [33].

For intermediate values of J, the measured dephasing rate exceeds contributions from Γ_ε and Γ_n for the single- and multielectron cases. The excess dephasing is well described by including a phenomenological additional dephasing rate Γ_0 that is independent of detuning. Fits to the data in Figs. 3(c) and 3(d) yield $\Gamma_0 = 14$ MHz for
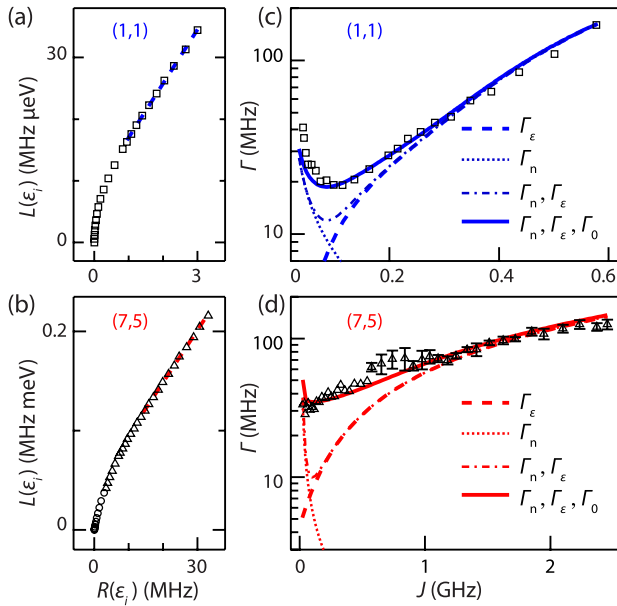
FIG. 3 (color online).   Plotting the left side integral $L(\varepsilon_i)$ versus the right side integral $R(\varepsilon_i)$ of Eq. (4) allows us to extract a rms ε noise of (a) $\delta\varepsilon = 2.0$ μeV for (1,1) and (b) $\delta\varepsilon = 1.2$ μeV for (7,5) dot occupations (dashed lines). Deviations from linear behavior indicate the presence of non-ε noise. Using the extracted values for $dJ/d\varepsilon$ and $\delta\varepsilon$, the dephasing rate due to ε noise Γ_ε can be predicted without any free parameters. For both (c) (1,1) and (d) (7,5), the system is dominated by ε noise at large J, but decoheres due to an unknown source at small J. The excess dephasing rate is not explained by nuclei (Γ_n), but is well captured by a model (Γ_Σ) that includes a constant dephasing rate Γ_0 as its only free parameter (see text).

FIG. 4 (color online).   (a) Quality of exchange rotations Q as a function of J for (7,5) and (1,1). For large J, the multielectron exchange gate significantly outperforms the single-electron gate. The model (solid lines) includes dephasing due to ε noise, nuclei, and a constant Γ_0 to account for the unknown noise source discussed in Fig. 3. Also shown (dotted lines) are the same models without the contribution from Γ_0. (b) The observed reduction of Q when applying external voltage fluctuations of fixed amplitude δV_{ext} to the detuning axis is in good agreement with the model including Γ_0 (solid line), and is in disagreement with the model excluding Γ_0 (dotted line). All model parameters determined from other measurements. This serves as an independent check of our model parameters.

the single-electron case and $\Gamma_0 = 34$ MHz for the multielectron case.

We take the total dephasing rate, $\Gamma_\Sigma = (\Gamma_\varepsilon^2 + \Gamma_n^2 + \Gamma_0^2)^{1/2}$, as the quadrature sum of these contributions. Strictly speaking, nuclear noise and electrical noise should not be combined in quadrature because the exchange oscillation is not separable into nuclear and electrical contributions. However, we have verified numerically that this introduces a small error. Figure 4(a) compares the quality factor Q of exchange oscillations with the model value $J\Gamma_\Sigma$. The agreement between model and experiment is excellent in both the single- and multielectron regimes. Model calculations shown in the insets of Figs. 1(c) and 1(d), also use these parameters.

The additional rate Γ_0 cannot be readily explained by higher-frequency electrical noise, as whitening the noise power spectrum would presumably increase dephasing for short exchange pulses. This would tend to increase dephasing at large J, opposite of the observed trend. As in [25], we observed no significant temperature dependence of quality factors when heating the mixing chamber from below 50 to 200 mK.

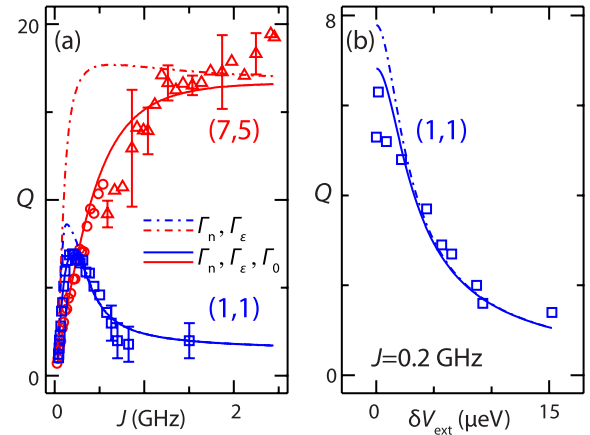As a check of our noise model, we use the plunger gates to artificially expose the quantum dots to a known electrical noise environment and observe its effect on the quality of exchange rotations. A two-channel arbitrary waveform generator (Agilent 33522A) can emulate different noise spectra, as well as different noise correlations between right and left plunger voltages, that can be superimposed to the control voltages during the exchange pulse. To simulate ε-equivalent noise, we add anticorrelated voltage fluctuations of increasing rms amplitude to V_L and V_R, and observe exchange oscillations of decreasing quality factor. Figure 4(b) shows the expected decrease in Q for single-dot occupation at $J = 0.2$ GHz [34], in good agreement with the predictions from our noise model (solid line, no free parameters).

In conclusion, we have compared noise-sensitive exchange oscillations in single- and multielectron spin qubits. The multielectron dots are subject to less exchange noise than single-electron dots both because of a lowered noise susceptibility, $dJ/d\varepsilon$, and a lower rms noise value, $\delta\varepsilon$. Our observation of high-quality exchange oscillations between multiply occupied dots suggests a route to simplifying device fabrication while simultaneously improving performance. We speculate that the unknown dephasing source may be due to transverse electric fields effecting the tunnel coupling of the device, something that is not explicitly accounted for in the noise model. Future studies will investigate how improved performance depends on electron occupancy over a much broader range of occupancies.

[1] D. Loss and D. P. DiVincenzo, Phys. Rev. A **57**, 120 (1998).

[2] J. R. Petta, A. C. Johnson, J. M. Taylor, E. A. Laird, A. Yacoby, M. D. Lukin, C. M. Marcus, M. P. Hanson, and A. C. Gossard, Science **309**, 2180 (2005).

[3] H. Bluhm, S. Foletti, I. Neder, M. Rudner, D. Mahalu, V. Umansky, and A. Yacoby, Nat. Phys. **7**, 109 (2010).

[4] M. D. Shulman, O. E. Dial, S. P. Harvey, H. Bluhm, V. Umansky, and A. Yacoby, Science **336**, 202 (2012).

[5] E. A. Laird, F. Pei, and L. P. Kouwenhoven, Nat. Nanotechnol. **8**, 565 (2013).

[6] S. Nadj-Perge, S. M. Frolov, E. P. A. M. Bakkers, and L. P. Kouwenhoven, Nature (London) **468**, 1084 (2010).

[7] K. D. Petersson, L. W. McFaul, M. D. Schroer, M. Jung, J. M. Taylor, A. A. Houck, and J. R. Petta, Nature (London) **490**, 380 (2012).

[8] J. W. G. van den Berg, S. Nadj-Perge, V. S. Pribiag, S. R. Plissard, E. P. A. M. Bakkers, S. M. Frolov, and L. P. Kouwenhoven, Phys. Rev. Lett. **110**, 066806 (2013).

[9] B. M. Maune, M. G. Borselli, B. Huang, T. D. Ladd, P. W. Deelman, K. S. Holabird, A. A. Kiselev, I. Alvarado-Rodriguez, R. S. Ross, A. E. Schmitz, M. Sokolich, C. A. Watson, M. F. Gyure, and A. T. Hunter, Nature (London) **481**, 344 (2012).

[10] J. J. Pla, K. Y. Tan, J. P. Dehollain, W. H. Lim, J. J. L Morton, D. N. Jamieson, A. S. Dzurak, and A. Morello, Nature (London) **489**, 541 (2012).

[11] Fabrication yield for gate-defined dots is above 0.9 for established recipes. Tuning multidot devices to the single-electron regime has lower yield, ~0.5 per dot, due to disorder and unoptimzed gate designs. Tuning to the few (5–10) electron regime is highly reliable, with yield above 0.9.

[12] P. W. Brouwer, Y. Oreg, and B. I. Halperin, Phys. Rev. B **60**, R13977 (1999).

[13] X. Hu and S. Das Sarma, Phys. Rev. A **64**, 042312 (2001).

[14] S. Vorojtsov, E. R. Mucciolo, and H. U. Baranger, Phys. Rev. B **69**, 115329 (2004).

[15] A. C. Johnson, J. R. Petta, C. M. Marcus, M. P. Hanson, and A. C. Gossard, Phys. Rev. B **72**, 165308 (2005).

[16] S. Amaha, T. Kodera, T. Hatano, K. Ono, Y. Tokura, S. Tarucha, J. A. Gupta, and D. G. Austing, J. Phys. Soc. Jpn. **80**, 023701 (2011).

[17] H. O. H Churchill, A. J. Bestwick, J. W. Harlow, F. Kuemmeth, D. Marcos, C. H. Stwertka, S. K. Watson, and C. M. Marcus, Nat. Phys. **5**, 321 (2009).

[18] M. R. Buitelaar, J. Fransson, A. L. Cantone, C. G. Smith, D. Anderson, G. A. C. Jones, A. Ardavan, A. Khlobystov, A. A. R. Watt, K. Porfyrakis, and G. A. D. Briggs, Phys. Rev. B **77**, 245439 (2008).

[19] F. Pei, E. A. Laird, G. A. Steele, and L. P. Kouwenhoven, Nat. Nanotechnol. **7**, 630 (2012).

[20] Y. Hu, F. Kuemmeth, C. M. Lieber, and C. M. Marcus Nat. Nanotechnol. **7**, 47 (2011).

[21] G. Yamahata, T. Kodera, H. O. H. Churchill, K. Uchida, C. M. Marcus, and S. Oda, Phys. Rev. B **86**, 115322 (2012).

[22] J. Medford, Ł. Cywiński, C. Barthel, C. M. Marcus, M. P. Hanson, and A. C. Gossard, Phys. Rev. Lett. **108**, 086802 (2012).

[23] D. J. Reilly, J. M. Taylor, E. A. Laird, J. R. Petta, C. M. Marcus, M. P. Hanson, and A. C. Gossard, Phys. Rev. Lett. **101**, 236803 (2008).

[24] K. D. Petersson, J. R. Petta, H. Lu, and A. C. Gossard, Phys. Rev. Lett. **105**, 246804 (2010).

[25] O. E. Dial, M. D. Shulman, S. P. Harvey, H. Bluhm, V. Umansky, and A. Yacoby Phys. Rev. Lett. **110**, 146804 (2013).

[26] E. Barnes, J. P. Kestner, N. T. Nguyen, andS. Das Sarma, Phys. Rev. B **84**, 235309 (2011).

[27] E. Nielsen, E. Barnes, J. P. Kestner, and S. D. Sarma, Phys. Rev. B **88**, 195131 (2013).

[28] S. Mehl and D. P. DiVincenzo, Phys. Rev. B **88**, 161408 (2013).

[29] C. Barthel, D. J. Reilly, C. M. Marcus, M. P. Hanson, and A. C. Gossard, Phys. Rev. Lett. **103**, 160503 (2009).

[30] W. A. Coish and D. Loss, Phys. Rev. B **72**, 125337 (2005).

[31] J.-T. Hung, Ł. Cywiński, X. Hu, and S. Das Sarma, Phys. Rev. B **88**, 085314 (2013).

[32] See Supplemental Material at http://link.aps.org/supplemental/10.1103/PhysRevLett.112.026801 for charge sensing and single-shot readout, justification of Gaussian envelopes, nuclear T_2^*, full decoherence model, high-frequency single-electron exchange oscillations, and exchange oscillations from device 2.

[33] A. P. Higginbotham, F. Kuemmeth, M. P. Hanson, A. C. Gossard, and C. M. Marcus, unpublished.

[34] For Fig. 4(b), the Agilent 33522A waveform generator was programmed to output a 5 MHz sine wave (i.e., $\ll J$), phase modulated at 19 kHz.